JGR Space Physics

RESEARCH ARTICLE
10.1029/2020JA028755

Special Section:
Probing the Magnetosphere through Magnetoseismology and Ultra-Low-Frequency Waves

# The Combined Influence of Lower Band Chorus and ULF Waves on Radiation Belt Electron Fluxes at Individual *L*-Shells

**Laura E. Simms[1], Mark J. Engebretson[1], Craig J. Rodger[2], Stavros Dimitrakoudis[3], Ian. R. Mann[3], and Peter J. Chi[4]**

[1]Augsburg University, Minneapolis, MN, USA, [2]University of Otago, Dunedin, New Zealand, [3]University of Alberta, Edmonton, Canada, [4]UCLA, Los Angeles, CA, USA

**Key Points:**

- VLF and ULF waves are associated with same day electron (>1.5 MeV) decreases but with flux enhancement 1–2 days later
- ULF waves are nearly always more influential than chorus, but electron enhancement is most effective when both wave types are present
- Both VLF and ULF waves are more influential at *L* 4–6 than at lower altitudes

**Correspondence to:**
L. E. Simms,
simmsl@augsburg.edu

**Citation:**
Simms, L. E., Engebretson, M. J., Rodger, C. J., Dimitrakoudis, S., Mann, I. R., & Chi, P. J. (2021). The combined influence of lower band chorus and ULF waves on radiation belt electron fluxes at individual *L*-shells. *Journal of Geophysical Research: Space Physics*, *126*, e2020JA028755. https://doi.org/10.1029/2020JA028755

Received 27 SEP 2020
Accepted 14 APR 2021



**Abstract** We investigate the timing and relative influence of VLF in the chorus frequency range observed by the DEMETER spacecraft and ULF wave activity from ground stations on daily changes in electron flux (0.23 to over 2.9 MeV) observed by the HEO-3 spacecraft. At each *L*-shell, we use multiple regression to investigate the effects of each wave type and each daily lag independent of the others. We find that reduction and enhancement of electrons occur at different timescales. Chorus power spectral density and ULF wave power are associated with immediate electron decreases on the same day but with flux enhancement 1–2 days later. ULF is nearly always more influential than chorus on both increases and decreases of flux, although chorus is often a significant factor. There was virtually no difference in correlations of ULF Pc3, Pc4, or Pc5 with electron flux. A synergistic interaction between chorus and ULF waves means that enhancement is most effective when both waves are present, pointing to a two-step process where local acceleration by chorus waves first energizes electrons which are then brought to even higher energies by inward radial diffusion due to ULF waves. However, decreases in flux due to these waves act additively. Chorus and ULF waves combined are most effective at describing changes in electron flux at >1.5 MeV. At lower *L* (2–3), correlations between ULF and VLF (likely hiss) with electron flux were low. The most successful models, over $L = 4–6$, explained up to 47.1% of the variation in the data.

**Plain Language Summary** Low-frequency electromagnetic waves in the Earth's radiation belt are associated with immediate (same day) decreases in the electron population, but appear to increase the number of electrons 1–2 days later. This is most prominent in the outer radiation belt, at an equatorial distance of 4–6 Earth radii.

## 1. Introduction

Both chorus and ULF Pc5 waves are thought to influence electron flux levels, increasing them in some situations and decreasing them in others. Observations of single storms show that interactions with chorus can scatter electrons into the loss cone (Clilverd et al., 2016; Horne & Thorne, 2003; Shprits et al., 2007, 2008; Thorne et al., 2005) while ULF Pc5 waves can lead to loss through a combination of outward radial diffusion and magnetopause shadowing (Katsavrias et al., 2015; Kellerman & Shprits, 2012; Loto'aniu et al., 2010; Mann et al., 2012; Ozeke et al., 2020; Turner et al., 2012). However, chorus may also result in flux enhancement through local acceleration (Horne et al., 2005; Katsavrias et al., 2015; Reeves, 2013; Shprits et al., 2008; Summers et al., 1998), while ULF Pc5 waves accelerate electrons through inward radial diffusion (e.g., Hao et al., 2019; Katsavrias et al., 2019; Mann et al., 2004) and direct interaction (Claudepierre et al., 2013; Hao et al., 2014; Zong et al., 2009, 2017).

Both wave types often occur simultaneously before or during changes in electron flux levels (Li et al., 2005). It requires further investigation to determine whether they contribute equally to electron flux levels. Katsavrias et al. (2015) found that over $L = 3–5$, the electron population above 300 MeV/G increased when both chorus (inferred from the ratio of precipitating to trapped electron fluxes using POES data in low Earth orbit) and ULF wave power were high, but depleted when only ULF wave activity was high. They interpreted this to mean that chorus was the dominant driver of electron acceleration, but ULF waves, via outward diffusion, resulted in depletion. In a different pair of storms, inferred chorus appeared to accelerate electrons to relativistic energies while ULF waves further accelerated this population to ultrarelativistic

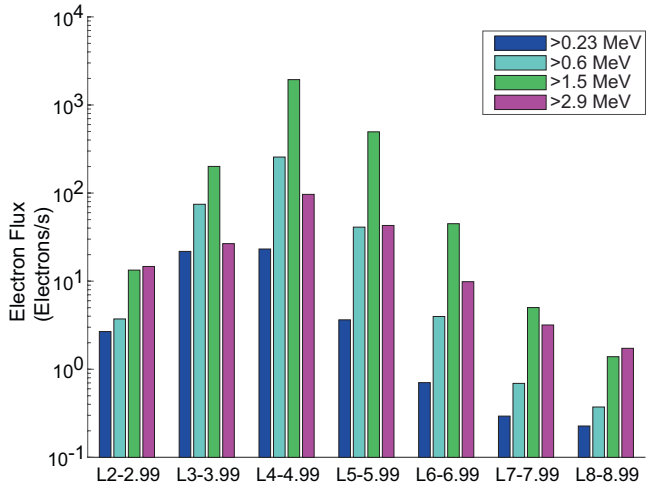


**Figure 1.** Mean daily electron fluxes at four energy ranges (>0.23, >0.6, >1.5, and >2.9 MeV) over $L$ = 2–9 (northern hemisphere).

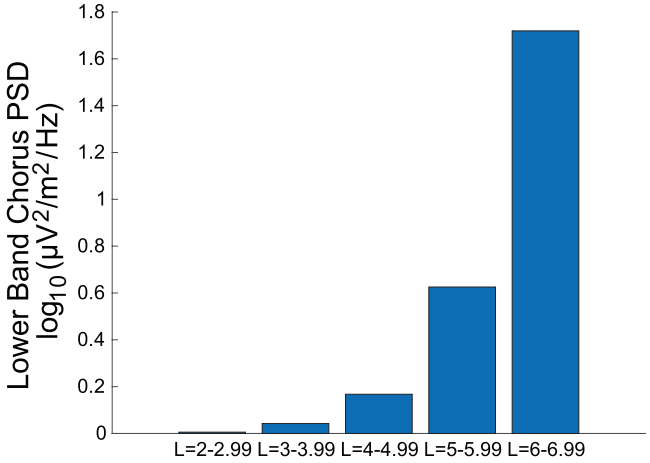


**Figure 2.** Mean daily lower band chorus PSD over $L$ = 2–6 (northern hemisphere). PSD, power spectral density.

energies through inward radial diffusion (Katsavrias et al., 2019). Using results from superposed epoch analysis, flux enhancements were associated with VLF activity (inferred from microbursts) around $L$ = 4.5, but at $L$-shells above that, the flux association was stronger with ULF activity (O'Brien et al., 2003). Analyzing effects simultaneously using multiple regression, ULF wave power at geosynchronous orbit was found to be of somewhat more influence on electron flux levels (>1.5 MeV) than satellite-observed chorus power spectral density (L. Simms et al., 2018; L. E. Simms et al., 2018).

There is, however, still a need to investigate these simultaneous wave effects by $L$-shell, over multiple days, using analyses which study the effect of each factor independent of the others. We use partial correlation analysis to study the influence of each wave type over several days. From these analyses, we are able to determine both when the waves are most influential, and to separate the positive and negative effects that occur on different days. Using multiple regression, we study the separate effects of each wave type on each day. We also explore the nonlinear action of waves on electron flux by including quadratic terms, and whether ULF and VLF waves act both additively and synergistically by including a multiplicative term (Neter et al., 1985).

In this study, we use electron flux data (HEO-3 satellite) gathered at each $L$-shell ($L$ = 2–8.99). We use satellite-observed VLF power spectral density (PSD) in the lower band chorus range from the DEMETER satellite, binned by $L$-shell over $L$ = 2–6.99. These waves are assumed to be predominately chorus above $L$ = 3 and predominately hiss below this (Bortnik et al., 2008; Carpenter & Park, 1973). This differs from previous studies of VLF correlation by $L$-shell with electron flux as the VLF measure is neither a proxy from microburst observation nor ground-based VLF data which does not as accurately reflect VLF wave activity occurring in space (Simms et al., 2019). We compare the effects of ULF Pc3, Pc4, and Pc5 data from ground-based stations, Pc5 from $L$ > 3.

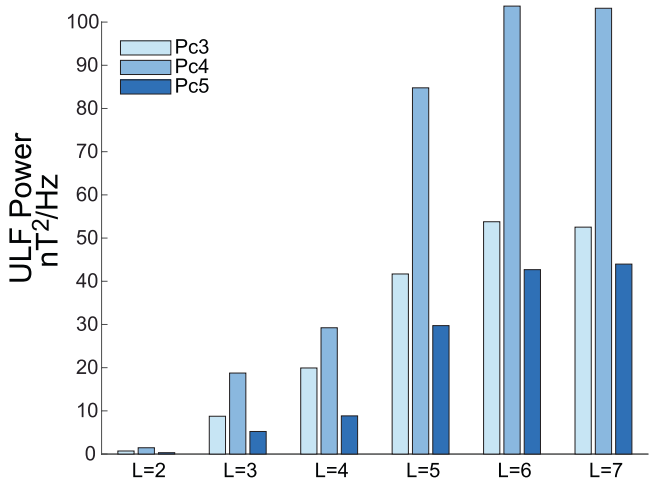


**Figure 3.** Mean daily ULF power (Pc3, Pc4, and Pc5) at McMAC stations BENN ($L$ = 2.5), GLYN ($L$ = 3.4), and CARISMA stations PINA ($L$ = 4.06), ISLL ($L$ = 5.15), GILL ($L$ = 6.15), and FCHU ($L$ = 7.44). BENN, Bennington; FCHU, Fort Churchill; GLYN, Glyndon, Island Lake; GILL, Gillam; PINA, Pinawa; ISLL.

**Table 1**
*Correlation of Same Day (Lag 0) and Previous Day (Lag 1) Hiss ($L \leq 3$) and Chorus ($L > 3$) PSD With >1.5 MeV Electron Flux Daily Change*

| *L*-Shell | Same day (lag 0) | Day previous (lag 1) |
|---|---|---|
| $L$ = 2–2.99 | 0.04 | 0.03 |
| $L$ = 3–3.99 | 0.07 | 0.15 |
| $L$ = 4–4.99 | −0.02 | 0.37 |
| $L$ = 5–5.99 | −0.02 | 0.35 |
| $L$ = 6–6.99 | −0.05 | 0.30 |

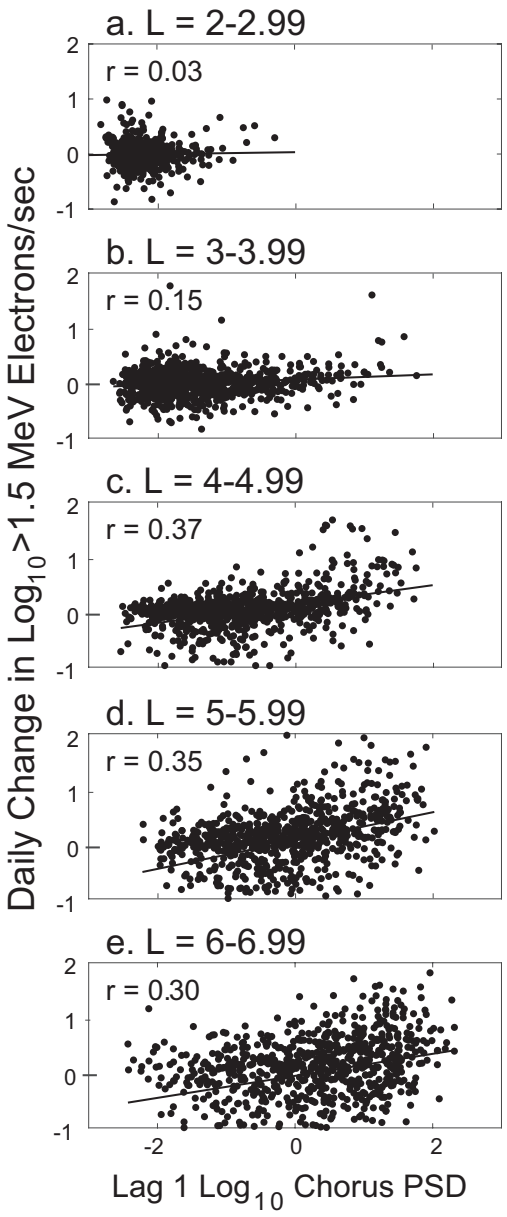


**Figure 4.** Scatterplots of mean daily lower band chorus $\log_{10}$PSD on previous day (Lag 1) versus daily change in >1.5 MeV $\log_{10}$electron flux channel over $L$ = 2–6 (a–e). The correlation coefficient ($r$) is given for each $L$. PSD, power spectral density.

## 2. Data and Statistical Methods

Data covered the time period August 11, 2004 to July 27, 2007. Electron flux data were obtained from the HEO-3 satellite which lies in a roughly 12 h highly elliptical orbit with good data coverage in the $L$ range from 2 to 9 (Fennell et al., 2004; Fennell & Roeder, 2008). The orbit is such that it cycles through all MLT. We use the E2 telescope channel (>0.23 MeV) and the omnidirectional sensors E4-E6 channels (>0.6, >1.5, and >2.9 MeV) (all sampling number of electrons/second) with observations binned by $L$-shell (IGRF) with, for example, $L$ = 2 including $L$ = 2.0–2.99. The E2 telescope temperature rose with altitude at $L \geq 5$ which increased noise levels. This may mean that results in the >0.23 MeV channel at higher $L$ are less reliable. We use only data collected over the northern hemisphere (high altitude) where dwell time at each $L$-shell is longer. This reduced variability in the data as pitch angles differ between northern and southern hemispheres. We did, however, retain both "even" and "odd" orbits, which sample different MLT, to obtain a more representative average of the electron population. Note that $L$ is correlated with latitude, with lower $L$-shells ($L \leq 3$) sampled from near the equator. As high energy protons can contaminate the electron channels, we removed days on which solar proton events were occurring, as well as one day following (ftp://ftp.swpc.noaa.gov/pub/indices/SPE.txt). However, there may also be proton contamination outside solar proton events. To correct for this, we removed data falling far above the cloud of data points when proton versus electron counts are plotted (O'Brien, 2012). This removed more lower $L$-shell observations ($L < 4$). For this reason, results from lower $L$-shells are not as robust.

We obtained power spectral density ($\log_{10}$ [$\mu V^2/m^2/Hz$]) of VLF waves (which may also be termed whistler mode waves) from dayside, northern hemisphere passes (LT 10:30) from the Instrument Champ Electrique (ICE) on the DEMETER satellite (Berthelier et al., 2006). There was good data coverage over $L$ = 2–6.99 (IGRF). We limit the VLF data to the lower band chorus range (0.1–0.5 fce). We use dayside VLF because it is found over a broader range of latitudes than nightside chorus and is not as influenced by geomagnetic activity (Agapitov et al., 2018; Li et al., 2009; Thorne et al., 2010; Tsurutani & Smith, 1977). However, this VLF wave band at lower $L$-shells (within the plasmasphere) is dominated by hiss (Bortnik et al., 2008). Chorus waves predominate above the plasmapause ($L \sim 3$) and hiss within the plasmasphere below this (Carpenter & Park, 1973). We therefore refer to these waves as hiss below $L$ = 3, chorus above that, and as the more general VLF when referring to both. This may represent only a sample of overall global activity as satellites can only sample one small area of the magnetosphere at a time. In particular, it may result in a certain $L$-shell being more heavily sampled at a particular local time. We note that the satellite data we use represent only a sample of overall global activity of the magnetosphere. In particular, due to the satellite orbit, each $L$-shell is only sampled at a particular latitude. This completely confounds the two variables in data sets from satellites that pass through several $L$-shells. It is possible, therefore, that differences seen at different $L$-shells are really the result of changing latitude, or to a combination of both $L$-shell and latitude.

ULF Pc3, Pc4, and Pc5 wave power ($nT^2/Hz$) was obtained from individual McMAC ground stations at $L$ = 2.5 (Bennington or BENN) and $L$ = 3.4

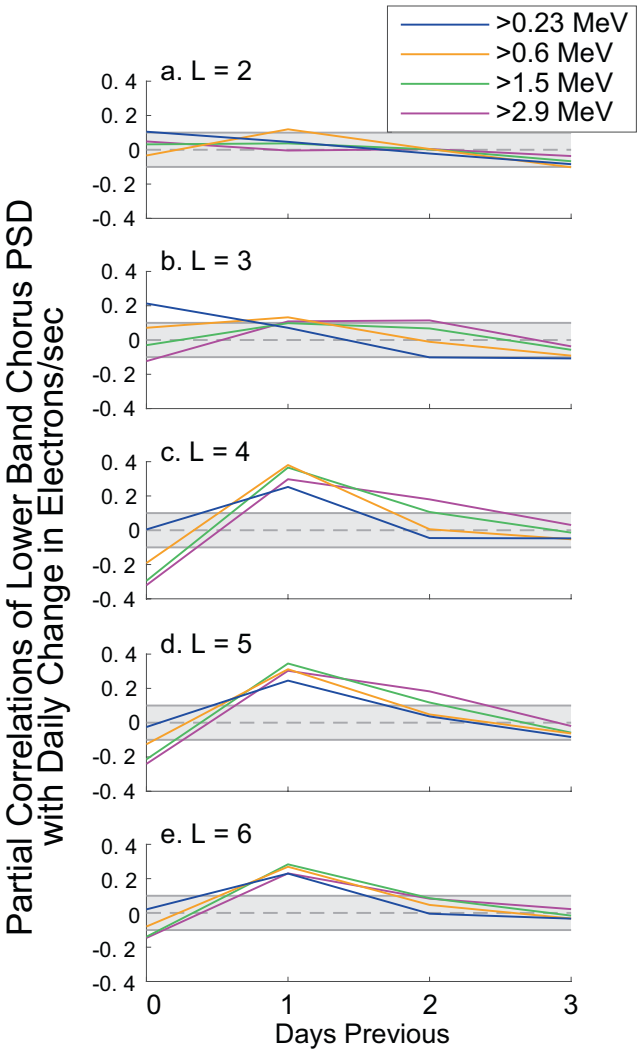


**Figure 5.** Partial correlations between mean daily lower band chorus $\log_{10}$PSD lagged over 0–3 days and daily change in four electron $\log_{10}$flux energy ranges (>0.23, >0.6, >1.5, and >2.9 MeV) over $L$ = 2–7 (a–f) (northern hemisphere). Correlations <0.10 lie within the gray area.

(Glyndon or GLYN) and CARISMA ground stations at $L$ = 4.06 (Pinawa or PINA), $L$ = 5.15 (Island Lake or ISLL), $L$ = 6.15 (Gillam or GILL), and $L$ = 7.44 (Fort Churchill or FCHU). Wave power was calculated using a Fourier transform with a 1 h window. This allows a good discernment of waves down to the minimum (Pc5) frequency of 1.67 mHz. There were strong correlations between the 3 ULF wave bands at all the ground stations, and each band correlated extremely similarly with electron flux. In order to compare most easily to the ULF index, we use Pc5 in most of our analyses, however, given the high correlations between bands, each of Pc3, Pc4, and Pc5 are a nearly identical proxy for the other two. Daily averaged ULF Pc5 wave power was obtained from a ground-based ULF Pc5 index covering local times 05:00–15:00 in the Pc5 range (2–7 mHz) obtained from magnetometers stationed at 60°–70°N CGM (Corrected GeoMagnetic) latitude (Kozyreva et al., 2007).

The log values of lower band chorus PSD, ULF power, and flux data were all daily averaged. Predictor variables (VLF and ULF wave activity) were lagged at 0 (same day; Lag 0), 1 (previous day; Lag 1), 2, and 3 days as most of the correlation between these waves and electron flux occurs within this time frame (Mann, O'Brien, & Milling, 2004; L. Simms et al., 2018). (Note that the Lag 3 waves occur first, with the Lag 0 waves occurring last, on the day of the flux measurement.) For the correlation and regression analyses, daily change in electron flux was calculated by subtracting the daily average of the previous day from the current day's average. All single correlations reported are standard Pearson correlation coefficients. Partial correlation between two factors fixes other variables at a given level to control for their effects (Neter et al., 1985).

The flux observations show serial autocorrelation ($p < 0.0001$ using Durbin-Watson test, see Neter et al., 1985), as each day is correlated with the previous day. To correct for this, we include previous day's flux as a predictor in the regression models. The addition of the AR1 term reduces the autocorrelation enough that we can have confidence in the p-values of the statistical tests. The result of this is that the regressions are essentially AR1 (autoregressive at one time step, represented by the previous day's flux term) differenced (as the observations are daily change) distributed lag transfer function models (Hyndman & Athanasopoulos, 2018; Simms et al., 2019). The addition of a predictor measured on several days previous (the distributed lags) allows this model to assess the effect of that predictor over time rather than all at once. Nonlinear effects of waves

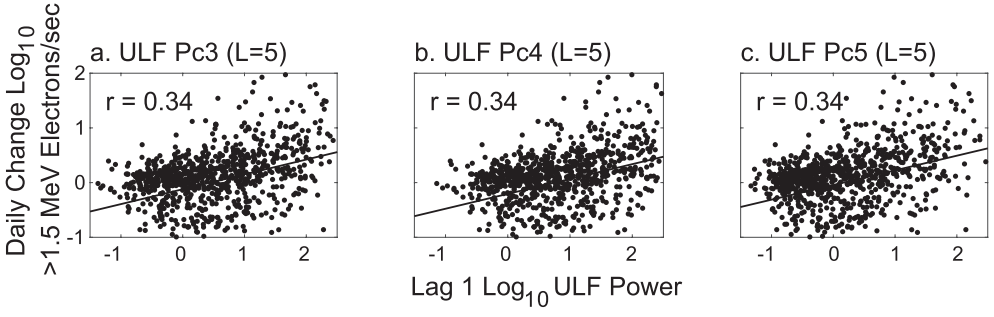


**Figure 6.** Scatterplots of ULF power (Lag 1) and >1.5 MeV electron flux at $L$ = 5. (a) ULF Pc3, (b) ULF Pc4, (c) ULF Pc5. All ULF bands show nearly identical correlations with flux.

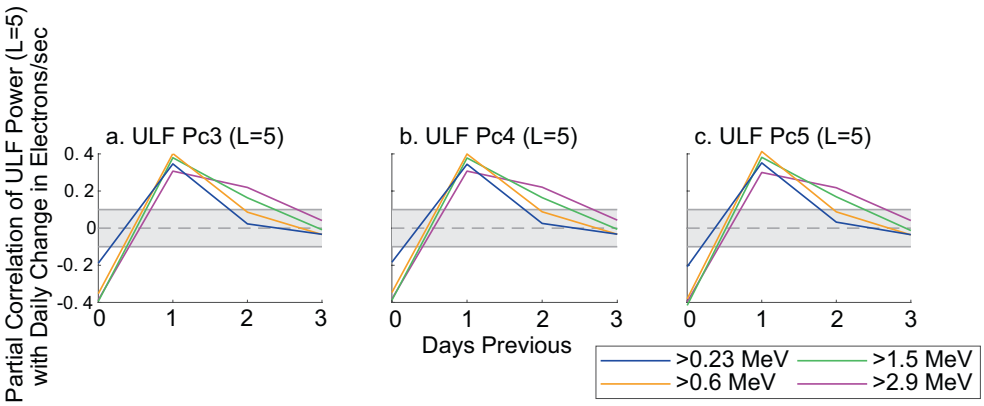


**Figure 7.** Partial correlations at $L = 5$ between mean daily ULF (a) Pc3, (b) Pc4, and (c) Pc5 over 0–3 days previous and daily change in 4 electron $\log_{10}$flux energy ranges (>0.23, >0.6, >1.5, and >2.9 MeV).

on electron flux are explored by including quadratic terms in the regression analyses, while the synergistic combined action of ULF and VLF waves is tested by including a multiplicative term (Neter et al., 1985).

We note that these data are only observational. Without the ability to randomly set the independent predictor variables in space physics studies, we are unable to infer causality, merely associations between variables. Strictly speaking, we should only refer to these correlations as associations, however for ease of discussion of the possible physical implications, we do refer to these, at times, as drivers or influences in order to fully explain the conclusions we make.

Statistical analyses were performed in MATLAB.

## 3. Results

Daily average electron fluxes peak at $L = 4$, with lower values observed in the slot region ($L = 2$) and beyond geosynchronous orbit ($L > 6$) (Figure 1). In contrast, $\log_{10}$ lower band chorus PSD (from DEMETER satellite) increases steadily up to $L = 6$ (Figure 2).

The power of all three ULF bands from the ground stations (Pc3, Pc4, and Pc5) rise over $L = 2$–6, with very low power seen at L2 (Figure 3). ULF Pc4 has the highest power, but there are such high correlations between these three bands (0.9432–0.9989) that any band is an almost exact proxy for the other two.

### 3.1. Correlations Between VLF PSD and Electron Flux

Neither hiss nor chorus PSD on the same day (Lag 0) is strongly associated with electron flux difference at >1.5 MeV with correlations ranging from −0.02 to 0.07 (Table 1). When chorus is measured the day before (Lag 1), there are stronger correlations at $L > 3$, but all are below 0.40 (Figure 4 and Table 1).

**Table 2**
*Correlation of Same Day (Lag 0) and Previous Day (Lag 1) ULF Pc5 Power With >1.5 MeV Electron Flux Daily Change*

| *L*-Shell | (a) Same day (lag 0) | (b) Day previous (lag 1) |
|---|---|---|
| $L = 2$ (BENN) | 0.05 | 0.06 |
| $L = 3$ (GLYN) | 0.06 | 0.19 |
| $L = 4$ (PINA) | −0.19 | 0.33 |
| $L = 5$ (ISLL) | −0.19 | 0.34 |
| $L = 6$ (GILL) | −0.20 | 0.30 |
| $L = 7$ (FCHU) | −0.20 | 0.18 |

Both hiss and flux differences show little spread below $L = 3$. Values are tightly clustered at low VLF PSD (not much VLF is seen at these *L*-shells) and around 0 change in electrons. This may reduce the likelihood of seeing much influence of the VLF mode waves on changes in electron flux at $L = 2$–2.99.

We perform partial correlations between VLF waves at each *L*-shell (2–6) over 0–3 days with daily flux difference at the four energy levels (Figure 5, $r < 0.10$ lie within the gray band). At $L = 2$–2.99 (hiss), nearly all correlation magnitudes were less than 0.1. Over $L = 4$–5, chorus measured on the same day is associated with a drop in flux at the 3 higher energies. Chorus measured one day before (Lag 1) is most associated with an increase in flux at all four energies over $L = 4$–6. However, none of

the correlations exceed 0.4. These low correlations suggest that the chorus is not the only driver of electron changes. However, we note that the partial correlation analysis differentiates the Lag 0 effect more clearly than the simple correlation analysis of Table 1. Over $L = 4$–5, at >1.5 MeV, electron reductions at Lag 0 due to chorus are stronger (L4: $r = -0.32$, L5: $r = -0.21$ in the partial correlations). The Lag 1 partial correlation with flux enhancement is more similar (L4: $r = 0.38$, L5: $r = 0.35$ in the >1.5 MeV partial correlations) to that found with simple correlation.

### 3.2. Correlations Between ULF Power and Electron Flux

Despite the obvious differences in power, extremely high correlations (0.9432–0.9989) between the three ULF bands (Pc3, Pc4, and Pc5) suggest that any one could serve as an excellent proxy for the others. Simple correlations between each ULF band (Lag 1) and >1.5 MeV electron flux at $L = 5$ are identical (Figure 6). Partial correlations over 0–3 days previous between ULF in each band with the daily differences in the four electron flux energies at $L = 5$ show this to be the case (Figure 7). The pattern of correlation was virtually the same between each ULF band and electron flux. These correlations were similarly indistinguishable at the other $L$-shells. We continue our analysis using ULF Pc5 data.

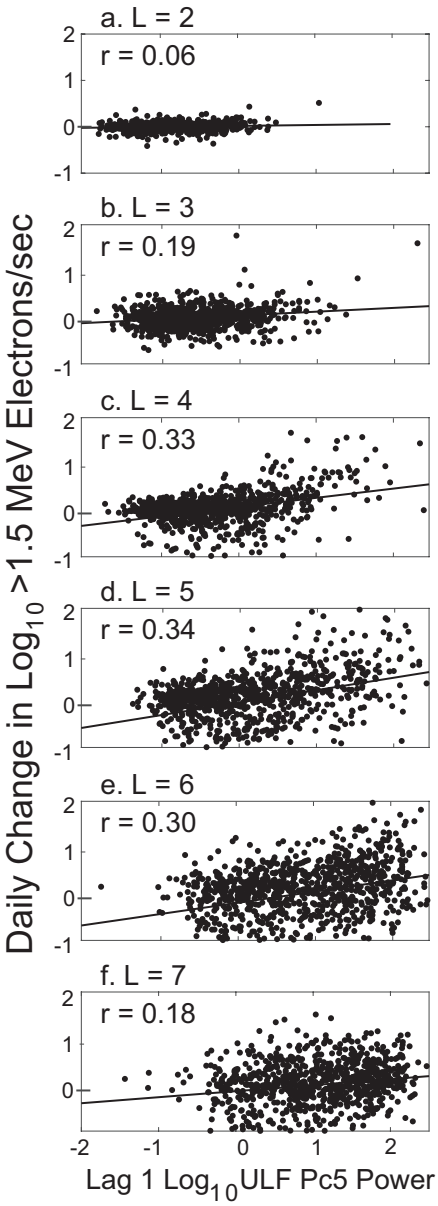


**Figure 8.** Scatterplots of mean daily ULF Pc5 $\log_{10}$ power on previous day (Lag 1) versus daily change in >1.5 MeV $\log_{10}$ electron flux channel over $L = 2$–7 (a–f). The correlation coefficient ($r$) is given for each L.

ULF power shows a similar pattern to that of the effect of chorus (or hiss at the lower $L$-shells) on >1.5 MeV flux: Lag 1 correlations tend to be positive and of greater magnitude than Lag 0 correlations. Both Lag 0 and Lag 1 correlations are greatest in magnitude over $L = 4$–7 (Table 2; Figure 8). ULF Pc5 at $L = 5$ is the most highly correlated ($r = 0.34$).

Partial correlations of ULF power at each $L$-shell (1–7) with the flux differences over 0–3 days lags show a similar pattern to that of VLF waves (Figure 9). At $L = 2$, all correlations were low (close to or less than|0.1|). At $L = 3$, the most important ULF correlations are at Lag 1, but these are all ≤0.25. Over $L = 4$–7, the peak in positive association occurs with previous day's ULF, while the strongest negative correlations are with Lag 0 ULF. Using partial correlation analysis, we can more clearly see the electron decreases at Lag 0 associated with ULF waves than the individual correlations of Table 2 would suggest. The middle range of flux energies (>0.6 and >1.5 MeV) show the highest response ($r$ as low as −0.4 at Lag 0 and as high as 0.4 at Lag 1). ULF power from 2 days previous is less associated with flux changes and that from 3 days prior is below |0.10|.

### 3.3. The ULF Index Is a Reasonable Proxy for ULF Pc5 Power at Each $L$-Shell

If ULF power measurements from each $L$-shell are not available, the ULF index can be a practical replacement. The correlation of the index with ULF Pc5 power at ground stations at each $L$-shell is reasonably high (0.74–0.85, Table 3a). The correlation of daily change of electron flux at each $L$-shell with the Lag one index is also very similar to that with each ground station, despite not being centered on a particular $L$-shell (compare Table 2b with Table 3b).

### 3.4. Combined Effects of Chorus and ULF Pc5

A key question is whether the two most important factors, chorus (at $L > 3$) and ULF Pc5, each still correlate with flux changes when the other factor is accounted for. To determine this, we perform multiple regres-

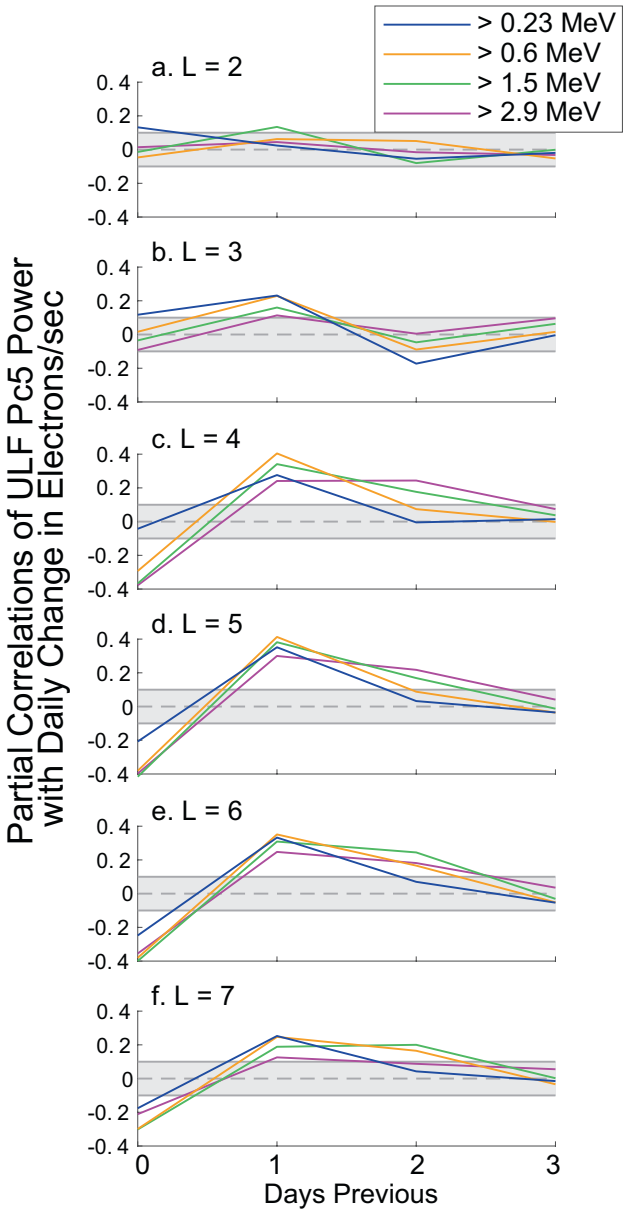


**Figure 9.** Partial correlations between mean daily ULF Pc5 lagged over 0–3 days and daily change in four electron $\log_{10}$flux energy ranges (>0.23, >0.6, >1.5, and >2.9 MeV) over $L$ = 2–7 (a–f). Correlations <0.10 lie within the gray area.

sions including both wave types, producing standardized regression coefficients so as to compare relative strengths of predictors on a common scale. As the highest partial correlations were on Lag 0–2 (same day to 2 days previous) we include all these measures over $L$ = 3–6, the $L$-shells in which both chorus and ULF power have good data coverage and where the individual correlations with flux were highest. Previous day's flux (Lag 1 daily flux change) is included as a predictor in the model to correct for serial autocorrelation (leading to an essentially AR1 model).

Over $L$ = 4–6, ULF Pc5 consistently shows a stronger influence than chorus over Lag 0–1, with a negative influence at Lag 0 and positive influence at Lag 1 (Figure 10; red line indicates statistically significant coefficients). It is notable that above 0.6 MeV the influence of ULF Pc5 Lag two increases from low to high flux energy levels, while that at Lag 1 decreases. This indicates that it takes up to several days for processes driven by these waves to accelerate electrons up to the higher energies. At the 3 highest energies, ULF Pc5 influence at each time step is strongest at $L$ = 4 (decreasing through $L$ = 6) and at >0.6 MeV flux (decreasing up to >2.9 MeV). At $L$ = 3, Lag 1 ULF is also much more important than chorus. However, there is more effect of chorus at Lag 0 at the higher two energies, and the ULF correlation is positive at the two lower energies.

This combined variable set (lags 0–2 of both chorus and ULF and previous day's flux) is most strongly associated with flux differences at >1.5 MeV. $R^2$ (percent of variability in the data explained by the regression model) peaks at 47.1% at $L$ = 5 in the >1.5 MeV energy range. This corresponds roughly to a correlation of 0.69 (the square root of $R^2$). However, the variability explained is not much lower at the other three energies. The rough correlation estimate is similar at >0.6 and > 2.9 MeV ($r$ = 0.66 and 0.65), but somewhat lower at >0.23 MeV (0.58). At each $L$-shell and energy, the correlation of flux with chorus and ULF Pc5 combined is higher than in the simple correlations. This indicates that both factors and all lags are needed for a fuller description of flux changes.

### 3.5. Nonlinear Effects of Chorus and ULF Pc5 on Flux

However, these linear, additive models may not completely capture the combined effects of chorus and ULF waves on electron flux. The effect of each factor may be neither linear nor independent of the other wave type. For each of Lag 0 and 1, we include squared terms to describe nonlinear effects, and a multiplicative interaction term to describe possible synergistic effects between the chorus and ULF wave effects. Regression surfaces show the predicted combined response of flux difference to both wave types with the marginal effects shown by the slope of the surface at each edge. The marginal effect is the effect of one predictor variable when the other predictor is held constant at 0.

When waves are measured on the same day as flux change (Lag 0) chorus and ULF waves appear to act independently. There is no strong multiplicative interaction visible in the surface plots (Figure 11). Over $L$ 4–5, at the three higher energies, the linear response to ULF power is negative with an increasingly negative response at higher ULF power (the nonlinear term). In contrast, at $L$ = 3, ULF is associated with flux increases, particularly at the lower energies. (This can also be seen in the regression coefficients of Figure 10.) The response to VLF waves is linear and positive over $L$ = 4–6.

However, a synergistic action is seen between wave types at Lag 1 at the three highest energies (Figure 12). Flux responds more positively to the highest chorus or ULF levels when the other wave type is also at a high

**Table 3**
*Correlation of the ULF Pc5 Index with Each Ground Station (L-Shell) and with Electron Flux*

| L-Shell | (a) ULF index with each ground station | (b) Electron flux with lag 1 ULF index |
|---|---|---|
| $L = 2$ | 0.74 | 0.05 |
| $L = 3$ | 0.83 | 0.19 |
| $L = 4$ | 0.85 | 0.38 |
| $L = 5$ | 0.80 | 0.33 |
| $L = 6$ | 0.78 | 0.24 |
| $L = 7$ | 0.76 | 0.13 |

*Note*. ULFcorrelation with (a) ULF Pc5 power at individual ground stations, and (b) with next day's >1.5 MeV electron flux daily change.

level. This can be seen on the surface plots in the unexpected rise in flux difference in the farthest corner (black arrows in 12b mark some of the strongest examples of this). However, as much of the chorus and ULF individual effects may be explained by their action within this multiplicative interaction term, the remaining individual marginal effects may appear negative (blue and orange arrows of Figure 12b). This is most notable with chorus and suggests that much of the positive effect of chorus is the result of joint action with ULF waves rather than from its own individual, additive effects. Increased electron flux, therefore, may be the result of a combination of processes driven by ULF and chorus waves. Flux enhancement is less likely to occur when either wave type occurs alone. Although the nonlinear component of chorus waves still tends to result in flux decreases, ULF waves show some positive, nonlinear effects, with the highest ULF power resulting in higher flux increases (green arrow of Figure 12b).

## 4. Discussion

In this study, we find that chorus and ULF waves are most explanatory of daily relativistic flux changes over $L = 4$–6, with their strongest influence seen on the >1.5 MeV electrons. Reductions and enhancements of flux due to these waves occur at different time scales, with decreases occurring nearly simultaneously (on the same day) with increased wave activity, while enhancement, particularly of higher energy electrons due to ULF waves, occurs over a longer time scale. In this scenario, waves drive electron acceleration beginning as early as 2 days before the flux measurement (Lag 2 wave measurement), with a peak in wave-driven acceleration 1 day before (at energies below 2.9 MeV). Then, at an immediate time scale (Lag 0), ULF and VLF waves may drive electron reductions. (However, we should note that because this is an observational study without randomly assigned levels of the predictors, we can only suggest direct causality. It is possible that Lag 1 waves prepare the magnetosphere to accelerate electrons via some other mechanism, or even that wave production and changes in electron population are both driven by another, unmeasured factor. This limitation in interpretation, however, is also shared by event-based studies.)

When measured on the same day as flux (Lag 0), chorus (above $L = 3$) and ULF waves predict electron decreases (at >0.6 MeV and above). There was little association between flux changes at higher energies and Lag 0 hiss (below $L = 4$), although we note a weak positive correlation at $L = 3$ in the >0.23 flux band. We assume these decreases may represent electron loss. This short timescale has been previously noted for VLF waves: loss due to scattering by chorus or hiss occurs at < 1 day (Summers et al., 2007) and within the plasmasphere (Jaynes et al., 2014).

However, when measured on the previous day (Lag 1), these waves are associated with flux enhancements on the following day, consistent with previous observations of chorus (at $L > 3$) and hiss (below $L = 3$) (Summers et al., 2007), as well as ULF influences on electron flux around 1 MeV (Elkington et al., 1999). Peak correlations between ULF waves and electron flux have been noted at a lag of 2–3 days (Mann et al., 2004). Our use of partial correlation analysis has refined the peak of the enhancement correlation to a 1 day lag by removing the loss influences that occur more immediately.

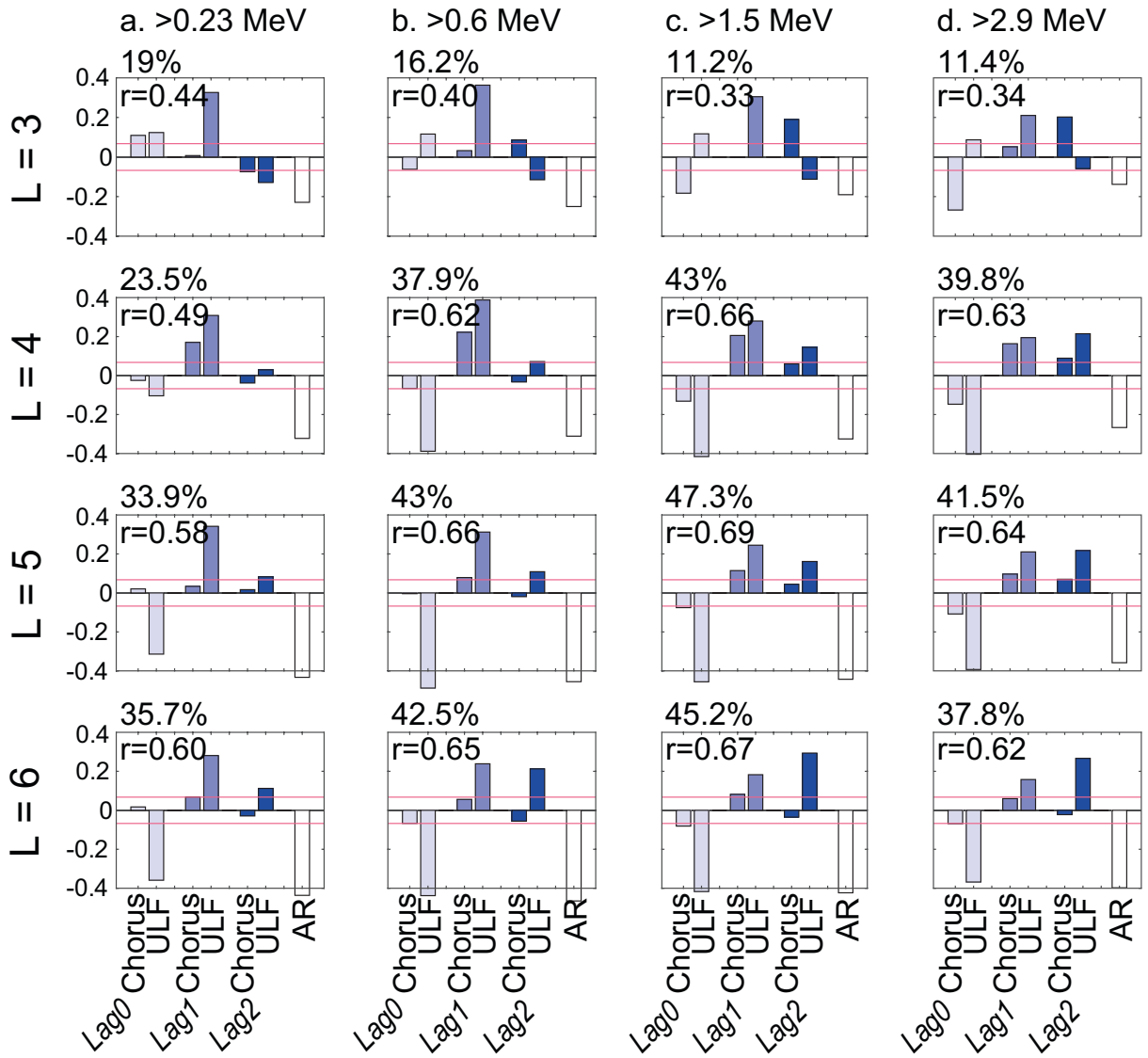


**Figure 10.** Standardized regression coefficients for each of $L$ = 3–6 predicting daily change in four electron flux energy ranges (a. >0.23, b. >0.6, c. >1.5, and d. >2.9 MeV) using lower band chorus PSD and ULF Pc5 power averaged over the same day (Lag 0; white), the previous day (Lag one; light blue), and 2 days previous (Lag two; dark blue) (northern hemisphere). Red lines denote statistically significant coefficients. Percent of variation in flux difference explained by the model is given at the top of each panel. This corresponds to the correlation ($r$) given within the panel. Lag one electron flux is added to each analysis to correct for serial autocorrelation. ULF at GLYN for $L$ = 3, PINA at $L$ = 4, ISLL at $L$ = 5, and GILL at $L$ = 6. GLYN, Glyndon; GILL, Gillam; ISLL, Island Lake; PINA, Pinawa; PSD, power spectral density.

Over $L$ = 4–6, ULF Pc5 wave activity from two days previous (Lag 2) is also influential at higher $L$-shells and/or at higher electron energies. At Lag 2 (waves measured two days before flux), above $L$ = 3, the influence of ULF Pc5 increases from low to high electron energy levels, while that of the Lag 1 response drops off. Enhancement processes due to ULF waves, therefore, appear to energize electrons in stages, bringing them from lower to the highest energies over a period of days, a response that has been noted previously in geomagnetic indices and solar wind speed (Rodger et al., 2010). This trend was seen for chorus influences as well over $L$ = 4–5, but it is much less marked. It is also notable that the Lag 2 ULF influence increases at higher $L$-shells, while the influence of VLF waves drops off. The implications of these trends are that inward radial diffusion, driven by ULF waves, takes some time (>1 day) to bring electrons to the higher energies, and that radial diffusion is of more importance at $L > 3$ with increasing influence at higher $L$-shells.

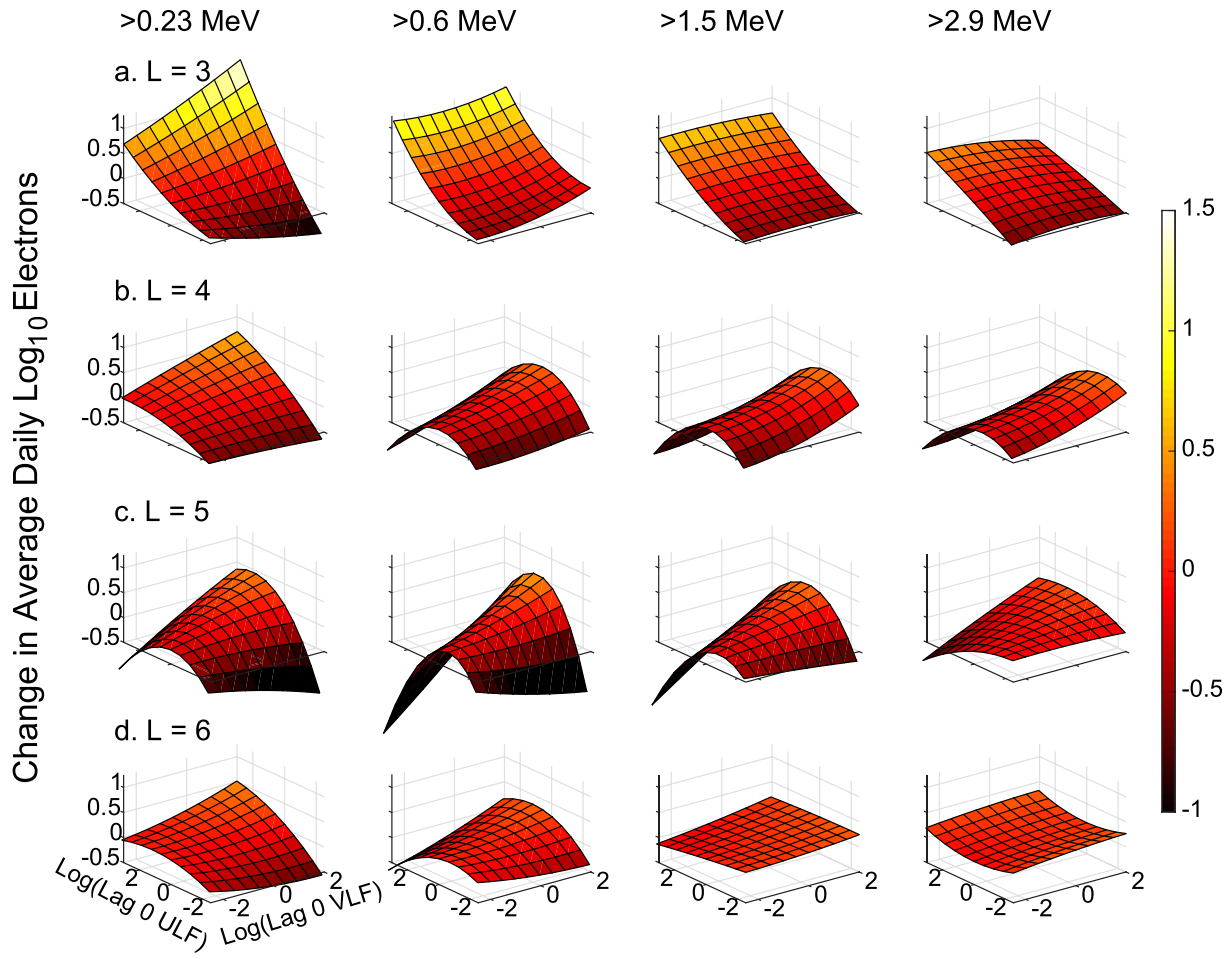


**Figure 11.** Predicting change in daily flux using linear and quadratic terms of Lag 0 $\log_{10}$(ULF Pc5 power) and chorus $\log_{10}$(PSD) as well as their multiplicative interaction term over $L = 3$–6 (a–d) at four flux energy ranges (>0.23, >0.6, >1.5, and >2.9 MeV). Lag one electron flux is added to each analysis to correct for serial autocorrelation. ULF at GLYN for $L = 3$, PINA at $L = 4$, ISLL at $L = 5$, and GILL at $L = 6$. GLYN, Glyndon; GILL, Gillam; ISLL, Island Lake; PINA, Pinawa; PSD, power spectral density.

We note that $L$-shell and latitude are confounded in the HEO-3 data set, resulting in a correlation between pitch angle and $L$-shell. As wave-particle interactions may depend on pitch angle, this may be at least part of the reason behind the correlational differences seen between flux changes and waves at different $L$-shells (Gannon et al., 2007; Shprits et al., 2008; West et al., 1973).

Previously, it was suggested that electron flux peaks are due to both VLF/ELF and ULF acceleration equally near $L = 4.5$, but to ULF acceleration alone at and above geosynchronous orbit (O'Brien et al., 2003). However, we have here found that the association of ULF waves with flux changes is stronger than that with VLF waves at all $L$-shells studied (at Lag 1). Although we note that the chorus (VLF) effect is strongest relative to the ULF correlation at $L = 4$, its standardized regression coefficient is still always less than the corresponding ULF coefficient. This difference in relative effect of VLF versus ULF between studies may result from our use of satellite-observed VLF data which is a more accurate depiction of chorus rather than the microburst proxy data used in the previous study. However, there are other differences. We do not analyze flux changes solely following storms, choosing instead to measure daily changes; we use multiple regression to statistically determine the simultaneous effects of VLF and ULF; and the levels of geomagnetic activity between our time period of study (2004–2007) and that of the previous paper (1996–2001) are dissimilar. All these differences may contribute to finding a stronger relative enhancement effect of ULF waves over $L = 3$–6.

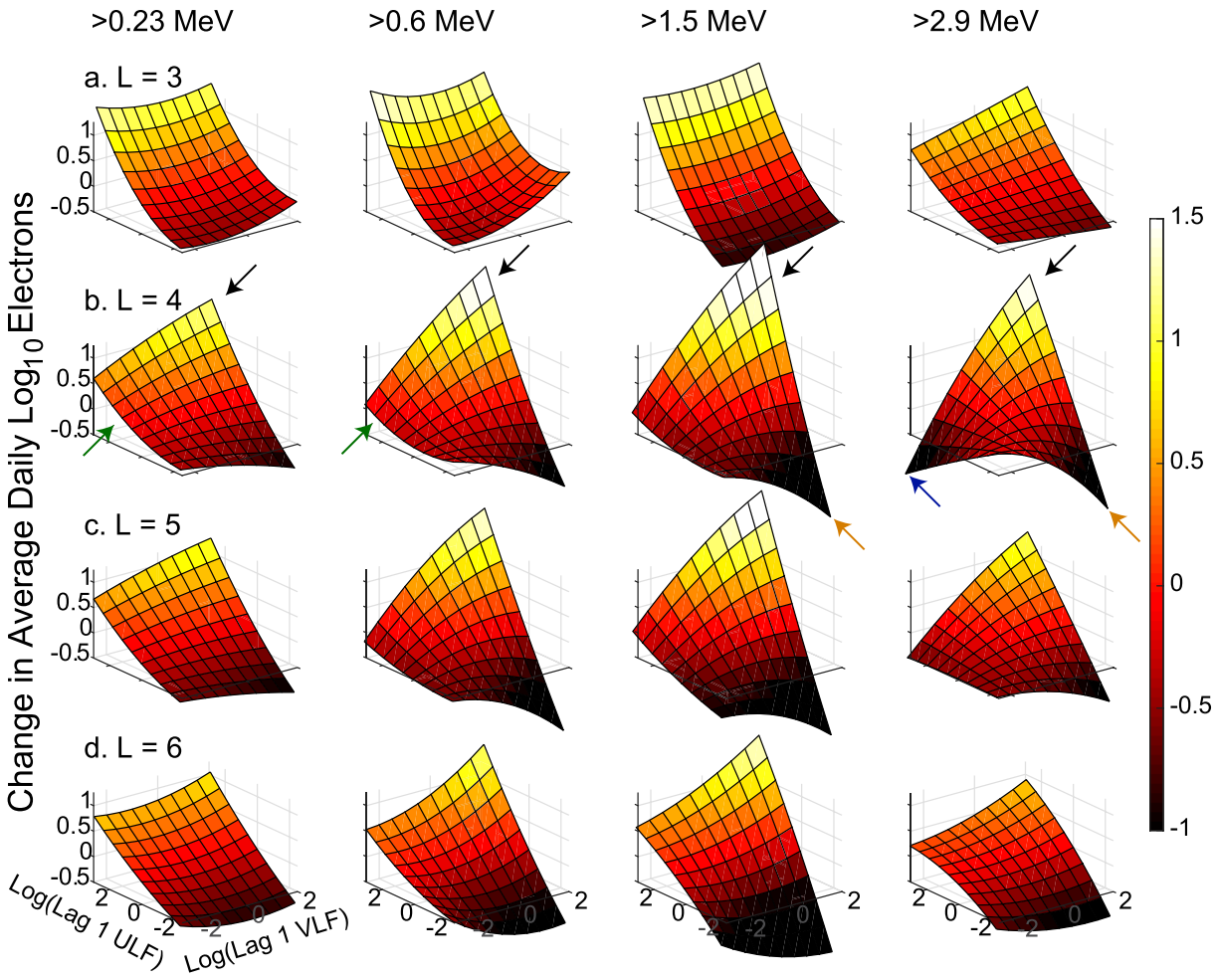


**Figure 12.** Predicting change in daily flux using linear and quadratic terms of Lag 1 $\log_{10}$(ULF Pc5 power) and chorus $\log_{10}$(PSD) as well as their multiplicative interaction term over $L = 4$–6 (a–d) at four flux energy ranges (>0.23, >0.6, >1.5, and >2.9 MeV). Black arrows indicate examples of strong multiplicative interaction; blue arrows are examples of ULF effect becoming negative at high ULF power when the ULF-VLF multiplicative interaction is strong; green arrows indicate nonlinear increased effect at high ULF power. Lag one electron flux is added to each analysis to correct for serial autocorrelation. ULF at GLYN for $L = 3$, PINA at $L = 4$, ISLL at $L = 5$, and GILL at $L = 6$. GLYN, Glyndon; GILL, Gillam; ISLL, Island Lake; PINA, Pinawa; PSD, power spectral density.

Above $L = 3$, electron decreases (at Lag 0) are more strongly associated with ULF Pc5 wave activity than with chorus. This has been previously observed in several storms (Katsavrias et al., 2015), but we show this with a statistical analysis here. We also show that there is some contribution to electron reductions from chorus, presumably due to scattering of electrons into the loss cone. The strongest effect of chorus on electron decreases occurs at the highest electron energy (>2.9 MeV), with the influence dropping at each higher $L$-shell.

### 4.1. Nonlinear Influences of ULF and VLF Wave Activity

While at Lag 1 the linear regression model shows ULF Pc5 wave power is more strongly associated with flux changes than chorus, the addition of nonlinear (quadratic) and interaction (multiplicative) terms describes a more nuanced relationship. Flux enhancement is more likely when both chorus and ULF waves are high. Their action is more effective in combination than when alone. This was found previously for electrons at geosynchronous orbit (L. E. Simms et al., 2018) but we now confirm this finding for lower $L$-shells. Not all associations between flux change and wave activity are linear when the multiplicative interaction term is included in the model, nor are they all positive. These marginal (individual) negative responses in the nonlinear models result from much of the flux response being tied up in the multiplicative interaction term.

They are what is left over after the more significant, and positive, interactive effect is accounted for. This argues that the processes associated with chorus (local acceleration) and those associated with ULF waves (inward radial diffusion) are both necessary to produce flux enhancements and do not act independently. This is consistent with the proposed two-step process where local acceleration by chorus waves first energizes electrons which are then brought to even higher energies by inward radial diffusion (Jaynes et al., 2015; Katsavrias et al., 2019; Zhao et al., 2019).

The same cannot be said for flux decreases on the same day (Lag 0 analyses; $L$ 4–6). In this case, chorus and ULF waves act independently. There is no strong multiplicative interaction visible in the surface plots. Those processes associated with loss due to chorus (which scatters electrons into the loss cone) and ULF waves (via outward radial diffusion) are able to operate independently. There is some nonlinearity to the flux response to ULF waves with a stronger decrease in flux at high ULF in the lowest energies and less decrease in flux at high ULF in the higher energies.

## 5. Summary

(a) We use multiple regression to control for the effects of other variables and to determine the timescale of electron decreases versus enhancement. By holding other factors constant in this way, we see that the individual effects on electron reductions and enhancements due to chorus and ULF waves are often stronger than it would appear from individual correlations
(b) Over $L = 4$–6 (4.0–6.99), both chorus and ULF Pc5 correlate with immediate electron decreases and delayed enhancement
(c) ULF waves consistently show a stronger influence on electron enhancement than do chorus waves. ULF power is also often more associated with immediate (same day) electron reductions than chorus
(d) There is a synergistic interaction between chorus and ULF wave activity on electron enhancement. This means that their combined effect is stronger than would be expected. This points to a two-step process of electron acceleration where local acceleration by chorus waves energizes electrons which are subsequently brought to even higher energies by inward radial diffusion
(e) However, chorus and ULF waves may drive electron decreases additively. In other words, the actions of the two wave types act independently
(f) Contributions of ULF Pc5 and hiss to electron decreases and enhancement are low below $L = 4$, and minimal at $L = 2$

## Data Availability Statement

HEO-3 satellite data are available at: http://virbo.org/HEO.CDPP data are available at https://cdpp-archive.cnes.fr/.CARISMA data are available at https://www.carisma.ca/carisma-data-repository. McMAC data can be accessed through the CDAWeb at https://cdaweb.sci.gsfc.nasa.gov/index.html/. The ULF Pc5 index is available at http://ulf.gcras.ru/plot_ulf.html.

**Acknowledgments**
The authors thank T.P. O'Brien for suggesting this study, advice, and for providing electron data from the HEO-3 satellite. The authors thank R. Gamble for preparing and J.-J. Berthelier for providing DEMETER ICE data, available at the CDPP (Center de données de la Physique des Plasmas). The suggestions of two anonymous reviewers greatly improved this manuscript. Work at Augsburg University was supported by NSF Grants AGS-1651263 and AGS-2013648.

## References

Agapitov, O., Mourenas, D., Artemyev, A., Mozer, F. S., Bonnell, J. W., Angelopoulos, V., et al. (2018). Spatial extent and temporal correlation of chorus and hiss: Statistical results from multipoint THEMIS observations. *Journal of Geophysical Research: Space Physics*, *123*, 8317–8330. https://doi.org/10.1029/2018JA025725

Berthelier, J. J., Godefroy, M., Leblanc, F., Malingre, M., Menvielle, M., Lagoutte, D., et al. (2006). ICE, the electric field experiment on DEMETER. *Planetary and Space Science*, *54*(5), 456–471. https://doi.org/10.1016/j.pss.2005.10.016

Bortnik, J., Thorne, R. & Meredith, N. (2008). The unexpected origin of plasmaspheric hiss from discrete chorus emissions. *Nature*, *452*, 62–66. https://doi.org/10.1038/nature06741

Carpenter, D. L., & Park, C. G. (1973). On what ionospheric workers should know about the plasmapause-plasmasphere. *Reviews of Geophysics*, *11*, 133–154. https://doi.org/10.1029/RG011i001p00133

Claudepierre, S. G., Mann, I. R., Takahashi, K., Fennell, J. F., Hudson, M. K., Blake, J. B., et al. (2013). Van Allen Probes observation of localized drift resonance between poloidal mode ultra-low frequency waves and 60 keV electrons. *Geophysical Research Letters*, *40*, 4491–4497. https://doi.org/10.1002/grl.50901

Clilverd, M. A., Rodger, C. J., Andersson, M., Verronen, P. T., & Seppälä, A. (2016). Chapter 14: Linkages between the radiation belts, polar atmosphere and climate: Electron precipitation through wave particle interactions. In G. Balasis, I. A. Daglis, & I.

R. Mann (Eds.), *Waves, particles and storms in geospace* (pp. 355–376). Oxford: Oxford University Press. http://doi.org/10.1093/acprof:oso/9780198705246.003.0015

S. R. Elkington, M. K. Hudson, A. A. Chan, (1999), Acceleration of relativistic electrons via drift-resonant interaction with toroidal-mode Pc-5 ULF oscillations, *Geophysical Research Letters*, *26*, 3273–3276. https://doi.org/10.1029/1999GL003659

Fennell, J. F., Blake, J. B., Friedel, R., & Kanekal, S. (2004). The Energetic electron response to magnetic storms: HEO satellite observations (Aerospace Rep. TR-2004(8570)-5).

Fennell, J. F., & Roeder, J. L. (2008). Storm time phase space density radial profiles of energetic electrons for small and large K values: SCATHA results. *Journal of Atmospheric and Solar-Terrestrial Physics*, *70*(14), 1760–1773. https://doi.org/10.1016/j.jastp.2008.03.014

Gannon, J. L., Li, X., & Heynderickx, D. (2007). Pitch angle distribution analysis of radiation belt electrons based on combined release and Radiation Effects Satellite Medium Electrons A data. *Journal of Geophysical Research*, *112*, A05212. https://doi.org/10.1029/2005JA011565

Hao, Y. X., Zong, Q.-G., Wang, Y. F., Zhou, X.-Z., Zhang, H., Fu, S. Y., et al. (2014). Interactions of energetic electrons with ULF waves triggered by interplanetary shock: Van Allen Probes observations in the magnetotail. *Journal of Geophysical Research: Space Physics*, *119*, 8262–8273. https://doi.org/10.1002/2014JA020023

Hao, Y. X., Zong, Q. G., Zhou, X. Z., Rankin, R., Chen, X. R., Liu, Y., et al. (2019). Global-scale ULF waves associated with SSC accelerate magnetospheric ultrarelativistic electrons. *Journal of Geophysical Research: Space Physics*, *124*, 1525–1538. https://doi.org/10.1029/2018JA026134

Horne, R. B., & Thorne, R. M. (2003). Relativistic electron acceleration and precipitation during resonant interactions with whistler-mode chorus. *Geophysical Research Letters*, *30*(10). https://doi.org/10.1029/2003GL016973

Horne, R. B., Thorne, R. M., Glauert, S. A., Albert, J. M., Meredith, N. P., & Anderson, R. R. (2005). Timescale for radiation belt electron acceleration by whistler mode chorus waves. *Journal of Geophysical Research*, *110*, A03225. https://doi.org/10.1029/2004JA010811

Hyndman, R. J., & Athanasopoulos, G. (2018). *Forecasting: Principles and practice* (2nd ed.). Melbourne: OTexts.

Jaynes, A. N., Baker, D. N., Singer, H. J., Rodriguez, J. V., Loto'aniu, T. M., Ali, A. F., et al. (2015). Source and seed populations for relativistic electrons: Their roles in radiation belt changes. *Journal of Geophysical Research: Space Physics*, *120*, 7240–7254. https://doi.org/10.1002/2015JA021234

Jaynes, A. N., Li, X., Schiller, Q. G., Blum, L. W., Tu, W., Turner, D. L., et al. (2014). Evolution of relativistic outer belt electrons during an extended quiescent period. *Journal of Geophysical Research: Space Physics*, *119*, 9558–9566. https://doi.org/10.1002/2014JA020125

Katsavrias, C., Daglis, I. A., Li, W., Dimitrakoudis, S., Georgiou, M., Turner, D. L., & Papadimitriou, C. (2015). Combined effects of concurrent Pc5 and chorus waves on relativistic electron dynamics. *Annales Geophysicae*, *33*, 1173–1181. https://doi.org/10.5194/angeo-33-1173-2015

Katsavrias, C., Sandberg, I., Li, W., Podladchikova, O., Daglis, I. A., Papadimitriou, C., et al. (2019). Highly relativistic electron flux enhancement during the weak geomagnetic storm of April-May 2017. *Journal of Geophysical Research: Space Physics*, *124*, 4402–4413. https://doi.org/10.1029/2019JA026743

Kellerman, A. C., & Shprits, Y. Y. (2012). On the influence of solar wind conditions on the outer-electron radiation belt. *Journal of Geophysical Research*, *117*, A05217. https://doi.org/10.1029/2011JA017253

Kozyreva, O., Pilipenko, V., Engebretson, M. J., Yumoto, K., Watermann, J., & Romanova, N. (2007). In search of a new ULF wave index: Comparison of Pc5 power with dynamics of geostationary relativistic electrons. *Planetary and Space Science*, *55*, 755–769. https://doi.org/10.1016/j.pss.2006.03.013

Li, L., Cao, J., & Zhou, G. (2005). Combined acceleration of electrons by whistler-mode and compressional ULF turbulences near the geosynchronous orbit. *Journal of Geophysical Research*, *110*, A03203. https://doi.org/10.1029/2004JA010628

Li, W., Thorne, R. M., Angelopoulos, V., Bortnik, J., Cully, C. M., Ni, B., et al. (2009). Global distribution of whistler-mode chorus waves observed on the THEMIS spacecraft. *Geophysical Research Letters*, *36*, L09104. https://doi.org/10.1029/2009GL037595

Loto'aniu, T. M., Singer, H. J., Waters, C. L., Angelopoulos, V., Mann, I. R., Elkington, S. R., & Bonnell, J. W. (2010). Relativistic electron loss due to ultralow frequency waves and enhanced outward radial diffusion. *Journal of Geophysical Research*, *115*, A12245. https://doi.org/10.1029/2010JA015755

Mann, I. R., Murphy, K. R., Ozeke, L. G., Rae, I. J., Milling, D. K., Kale, A. A., & Honary, F. F. (2012). The role of ultralow frequency waves in radiation belt dynamics. *Geophysical Monograph Series*, *199*, 69–92. https://doi.org/10.1029/2012GM001349

Mann, I. R., O'Brien, T. P., & Milling, D. K. (2004). Correlations between ULF wave power, solar wind speed, and relativistic electron flux in the magnetosphere: Solar cycle dependence. *Journal of Atmospheric and Solar-Terrestrial Physics*, *66*(2004), 187–198. https://doi.org/10.1016/j.jastp.2003.10.002

Neter, J., Wasserman, W., & Kutner, M. H. (1985). *Applied linear statistical models* (pp. 1127). Homewood, IL: Richard D. Irwin, Inc.

O'Brien, T. P., Lorentzen, K. R., Mann, I. R., Meredith, N. P., Blake, J. B., Fennell, J. F., et al. (2003). Energization of relativistic electrons in the presence of ULF power and MeV microbursts: Evidence for dual ULF and VLF acceleration. *Journal of Geophysical Research*, *108*(A8), 1329. https://doi.org/10.1029/2002JA009784

O'Brien, T. P. (2012). Data cleaning guidelines for AE-9/AP-9 datasets (Aerospace Rep. TOR-2012(1237)-4).

Ozeke, L. G., Mann, I. R., Dufresne, S. K. Y., Olifer, L., Morley, S. K., Claudepierre, S. G., et al. (2020). Rapid outer radiation belt flux dropouts and fast acceleration during the March 2015 and 2013 storms: The role of ULF wave transport from a dynamic outer boundary. *Journal of Geophysical Research: Space Physics*, *125*, e2019JA027179. https://doi.org/10.1029/2019JA027179

Reeves, G. D., Spence, H. E., Henderson, M. G., Morley, S. K., Friedel, R. H. W., Funsten, H. O., et al. (2013). Electron acceleration in the heart of the Van Allen radiation belts. *Science*, *341*, 991–994. https://doi.org/10.1126/science.1237743

Rodger, C. J., Clilverd, M. A., Green, J. C., & Lam, M. M. (2010). Use of POES SEM-2 observations to examine radiation belt dynamics and energetic electron precipitation into the atmosphere. *Journal of Geophysical Research*, *115*, A04202. https://doi.org/10.1029/2008JA014023

Shprits, Y. Y., Meredith, N. P., & Thorne, R. M. (2007). Parameterization of radiation belt electron loss timescales due to interactions with chorus waves. *Geophysical Research Letters*, *34*, L11110. https://doi.org/10.1029/2006GL029050

Shprits, Y. Y., Subbotin, D. A., Meredith, N. P., & Elkington, S. R. (2008). Review of modeling of losses and sources of relativistic electrons in the outer radiation belt II: Local acceleration and loss. *Journal of Atmospheric and Solar-Terrestrial Physics*, *70*, 1694–1713. https://doi.org/10.1016/j.jastp.2008.06.014

Simms, L. E., Engebretson, M. J., Clilverd, M. A., & Rodger, C. J. (2019). Ground-based observations of VLF waves as a proxy for satellite observations: Development of models including the influence of solar illumination and geomagnetic disturbance levels. *Journal of Geophysical Research: Space Physics*, *124*, 2682–2696. https://doi.org/10.1029/2018JA026407

Simms, L., Engebretson, M., Clilverd, M., Rodger, C., Lessard, M., Gjerloev, J., & Reeves, G. (2018). A distributed lag autoregressive model of geostationary relativistic electron fluxes: Comparing the influences of waves, seed and source electrons, and solar wind inputs. *Journal of Geophysical Research: Space Physics*, *123*, 3646–3671. https://doi.org/10.1029/2017JA025002

Simms, L. E., Engebretson, M. J., Clilverd, M. A., Rodger, C. J., & Reeves, G. D. (2018b). Nonlinear and synergistic effects of ULF Pc5, VLF chorus, and EMIC waves on relativistic electron flux at geosynchronous orbit. *Journal of Geophysical Research: Space Physics*, *123*, 4755–4766. https://doi.org/10.1029/2017JA025003

Summers, D., Ni, B., & Meredith, N. P. (2007). Timescales for radiation belt electron acceleration and loss due to resonant wave-particle interactions: 2. Evaluation for VLF chorus, ELF hiss, and electromagnetic ion cyclotron waves. *Journal of Geophysical Research*, *112*, A04207. https://doi.org/10.1029/2006JA011993

Summers, D., Thorne, R. M., & Xiao, F. (1998). Relativistic theory of wave-particle resonant diffusion with application to electron acceleration in the magnetosphere. *Journal of Geophysical Research*, *103*, 20487–20500. https://doi.org/10.1029/98JA01740

Thorne, R. M. (2010). Radiation belt dynamics: The importance of wave-particle interactions. *Geophysical Research Letters*, *37*, L22107. https://doi.org/10.1029/2010GL044990

Thorne, R. M., O'Brien, T. P., Shprits, Y. Y., Summers, D., & Horne, R. B. (2005). Timescale for MeV electron microburst loss during geomagnetic storms. *Journal of Geophysical Research*, *110*, A09202. https://doi.org/10.1029/2004JA010882

Tsurutani, B. T., & Smith, E. J. (1977). Two types of magnetospheric ELF chorus and their substorm dependences. *Journal of Geophysical Research*, *82*, 5112–5128. https://doi.org/10.1029/JA082i032p05112

Turner, D. L., Shprits, Y., Hartinger, M., & Angelopoulos, V. (2012). Explaining sudden losses of outer radiation belt electrons during geomagnetic storms. *Nature Physics*, *8*, 208–212. https://doi.org/10.1038/NPHYS2185

West, Jr, H. I., Walton, J. R., & Walton, J. R. (1973). Electron pitch angle distributions throughout the magnetosphere as observed on Ogo 5. *Journal of Geophysical Research*, *78*, 1064–1081. https://doi.org/10.1029/JA078i007p01064

Zhao, H., Baker, D. N., Li, X., Malaspina, D. M., Jaynes, A. N., & Kanekal, S. G. (2019). On the acceleration mechanism of ultrarelativistic electrons in the center of the outer radiation belt: A statistical study. *Journal of Geophysical Research: Space Physics*, *124*, 8590–8599. https://doi.org/10.1029/2019JA027111

Zong, Q.-G., Zhou, X.-Z., Wang, Y. F., Li, X., Song, P., Baker, D. N., et al. (2009). Energetic electron response to ULF waves induced by interplanetary shocks in the outer radiation belt. *Journal of Geophysical Research*, *114*, A10204. https://doi.org/10.1029/2009JA014393

Zong, Q., & Zhou, R. X. (2017). The interaction of ultra-low-frequency pc3-5 waves with charged particles in Earth's magnetosphere. *Reviews of Modern Plasma Physics*, *1*(1), 10. https://doi.org/10.1007/s41614-017-0011-4